PHYSICAL REVIEW A VOLUME 20, NUMBER 3 SEPTEMBER 1979

K-shell photoabsorption coefficients of O_2, CO_2, CO, and N_2O

D. M. Barrus, R. L. Blake, A. J. Burek,* K. C. Chambers,† and A. L. Pregenzer‡
University of California, Los Alamos Scientific Laboratory, Los Alamos, New Mexico 87545
(Received 29 January 1979)

The total photoabsorption coefficient has been measured from 500 to 600 eV around the K edge of oxygen in gases O_2, CO_2, CO, and N_2O by means of a gold continuum source and crystal spectrometer with better than 1-eV resolution. The cross sections are dominated by discrete molecular-orbital transitions below the K-edge energy. A few Rydberg transitions were barely detectable. Broad shape resonances appear at or above the K edge. Additional broad, weak features above the K edge possibly arise from shake up. The authors give quantitative results that have about 10% accuracy (3σ), except on the very strong peaks. All the measured features are discussed in relation to other related measurements and theory.

I. INTRODUCTION

Absorption structure around the K- and L-shell ionization thresholds in low Z elements has evoked considerable interest in recent years because of the observation of remarkably strong features both below and above the photoionization threshold energy. The structure has been revealed by a combination of x-ray and ultraviolet photoelectron spectroscopy, electron scattering, photoabsorption with synchrotron or bremsstrahlung continuum sources, and photoemission. Understanding of this structure is important not only for knowledge of the atomic physics in molecular and solid state environments but also for practical applications in spectroscopy where the structure critically affects measurements.[1]

No previous quantitative measurements have been made for the absorption structure around the oxygen K-edge of CO or N_2O. There have been quantitative measurements for O_2 and CO_2 which we have tried to extend and improve in results reported here.[2] Tabulated semiempirical absorption coefficients[3] are available, but should not be used near absorption edges of light elements because of the dramatic fluctuations that have now been observed and were not included in the tabulations. Qualitative results on the structure are available in the literature for carbon, nitrogen, and oxygen edges in several gases and compounds.[4-12] We present here quantitative results on oxygen 1s absorption in O_2, CO_2, CO, and N_2O gases. For reasons discussed in Sec. II our accuracy is not very good on strong linelike features but is good on the continuum at greater energies.

Nefedov[13] and Zimkina and Vinogradov[14] paved the way to interpretation of the observed resonancelike structures. Nefedov[13] introduced the concept of pseudopotential barriers to explain the presence of peaks at energies above the photoionization threshold. He also mentions the need for mixing of atomic orbitals into molecular orbitals to explain peaks below the ionization threshold. Zimkina and Vinogradov[14] brought out the importance of the role of neighboring atoms combined with symmetry of the molecule. Dehmer[15] put these ideas together in a picture of a "two-well potential." The potential hump between the two wells arises from electrons occupying orbitals relatively far out from the atom in question. This picture permits the existence of negative energy discrete states in either the inner or outer well and positive energy quasidiscrete states in the inner well. Thus one can get narrow lines below the continuum onset and broad lines above it. He then set out a qualitative application of how this picture can explain numerous absorption spectra not only of molecules but also of solids. Subsequently Dehmer and Dill[16] showed quantitatively that these ideas have application beyond the highly symmetric cases for which they were introduced and that centrifugal barriers rather than Coulomb barriers may be determining the distribution of oscillator strength in many cases. There may be cases where exchange forces also contribute to such barrier effects. The very strong line seen below the K-shell ionization limit in N_2 and similar molecular spectra is a consequence of a centrifugal barrier which concentrates the d-wave component of a π-type ionization channel. Similarly a continuum resonance was shown to arise from the scattering of the outgoing p wave by the anisotropic molecular potential into a range of l states, one or more of which may penetrate the centrifugal barrier and achieve overlap with the core orbitals. The calculations show considerable low-amplitude oscillation of the partial photoionization cross sections. These are the molecular counterpart of extended x-ray absorption fine structure (EXAFS).

II. EXPERIMENTAL METHOD

Bremsstrahlung radiation from solid targets in x-ray sources of our own design was used as a reference spectrum. The x-ray beam was passed through a Soller collimator of three arc minutes measured full width at half-maximum (FWHM) angular response, dispersed by rubidium acid phthalate (RAP) or potassium acid phthalate (KAP) crystals, and detected by a flow proportional counter. Vertical beam divergence was limited to a few degrees by the spectrometer geometry. The spectrometer was aligned by well known techniques.[17]

Gases used were 99.5% pure or better, except for N_2O which was 98%. The 2% impurity in N_2O was primarily air, so the only significant contamination would have been 0.25% O_2. The dominant O_2 peak in the mass absorption coefficient μ/ρ to be described in Sec. III, did not show up in the N_2O data. Thus we conclude that all gases had adequate purity to assure less than one percent error in μ/ρ.

Polypropylene windows were used on the detector, the gas cell, and the isolation window between the x-ray source and spectrometer chamber. An aluminum heat reflector about 2000 Å thick was evaporated onto the isolation window, which was located between the source and spectrometer vacuum chambers. The thin Al_2O_3 layer that naturally forms on a pure aluminum surface would have been stable during the measurements and would not have caused any false structure in the gas data. A gas cell 3.175 cm long was operated at about 15 torr for the quantitative results presented here. Because of the "thickness effect,"[18] we also made measurements at about the same pressure in a cell 0.3175 cm thick. Pressure in the cell was stabilized to about 0.1% and measured with a calibrated gauge to 0.13% accuracy. Temperature was recorded for each data run and never changed in excess of 3 K. Outward bowing of the polypropylene windows on the gas cell could have caused our determination of the column density ρx to be too small by at most 1% in the long cell and 10% in the short cell. The combined long cell uncertainty in ρx was 1% at the 2σ level (ρ is gas density and x is path length), but it is a directional uncertainty in the sense that our μ/ρ values could be 1% smaller than we tabulate because the gas cell length is the dominant factor.

When a continuum source is used for absorption measurements it is especially important to take precautions to eliminate radiation outside the energy of interest. This means one has to suppress higher-order reflections that could reach the detector. We operated the detector with 300 torr of methane to provide good efficiency at 550 eV and low efficiency at higher energies. A nichrome layer ~50 Å thick inside the window suppressed the low-energy tail of pulses from photoelectrons and permitted a pulse-height distribution with 55% FWHM resolution. As the spectrum was scanned from 500 to 600 eV, a pulse-height position controller was used to constantly keep the pulse-height distribution centered in the pulse-height selection window. Measurements without this control showed substantial differences. The differences were minimized by varying the anode voltage. Optimum results were obtained at 3 kV where all our measurements were then made. As the voltage was increased, the errors grew rapidly.

Fluorescence and scattered radiation from the gas cell were eliminated from direct access to the detector by an 8° FWHM honeycomb collimator just outside the detector window. Fluorescence in the gas itself would reenter the beam in the filtered scans, but the low fluorescence efficiency (10^{-2}) and small solid angle assure negligible error from this cause. Flourescence and scattering from the crystal holder were not negligible. These were measured explicitly for each run by means of a separate measurement with the detector 5° off the position for Bragg reflection. In regions of high absorption this correction amounted to one-third of the filtered beam signal for oxygen (the worst case). The relative magnitude of this correction is independent of beam intensity but does depend on source voltage. The 3-kV operating voltage was selected in part to reduce errors from this cause.

Initially a tantalum anode x-ray source was operated at 3 kV and 140 mA with just enough air cooling to keep the anode at a red glow. This provided a reasonably intense continuum source of x-rays whose low-energy tail was monotonic declining over the range of oxygen K absorption, about 500 to 600 eV. In spite of operation with ion pumping in the 10^{-9}-torr range and a hot anode, the spectrum still contained minor amounts of carbon and oxygen line radiation. Some of this line emission came from the mylar blades of the 3-arc min FWHM entrance Soller collimator and simply contributed to the reference beam. Line emissions from the source and collimator in any case did not significantly influence the results.

Subsequently the measurements were repeated with a gold anode, evaporated in the x-ray source housing at a vacuum of 1×10^{-8} torr and operated at 2×10^{-9} torr. A slow buildup of oxygen on the anode over days of operation was monitored but did not cause a significant error. All data reported here are from the gold anode operated at 3 kV and 500 mA. Measurements with tne tantalum anode

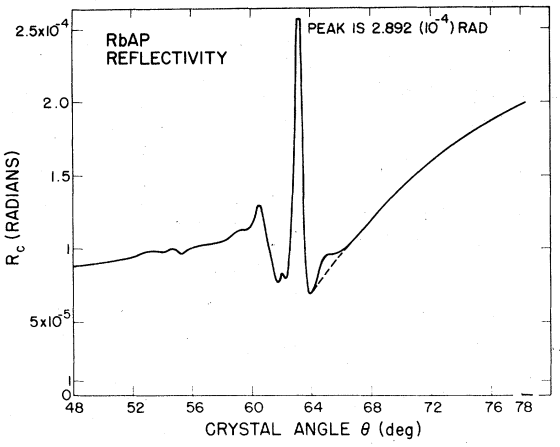

FIG. 1. Measured integrated coefficient of reflection R_c is plotted as a function of crystal angle when the crystal is used in a Bragg spectrometer arrangement with reflection from the (001) planes. The dashed line near 65° is the true R_c because the x-ray source had a small O $K\alpha$ contamination line that was not removed in the normalization procedure. The large variations are caused by the influence of the oxygen 1s absorption structure inside the crystal on the crystal structure factor. Interestingly this structure has the same kinds of variation that we found in the gases reported in this paper.

agree with the gold anode data but had poorer statistics.

Since the source spectrum is a continuum that is monotonic and slowly decreasing with decreasing energy, any structure seen in the reference spectrum without any absorber has to come from either windows in the beam or the crystal reflection coefficient. The polypropylene windows assured that only crystal problems would be involved. Unfortunately, the available crystals all contain oxygen, which causes the reflectivity to undergo large variations as a function of energy in the exact region of measurement. This phenomenon has been studied in detail and will be published separately. For present purposes we show in Fig. 1 the reflection coefficient R_c of the RAP crystal used for the absorption measurements. The reflection coefficient is plotted as a function of crystal angle to the incident beam. The photon energy varies from 640 eV at 48° to 486 eV at 78°. The large variations with photon energy almost exactly follow the absorption structure of oxygen inside the crystal.[19] These are not the structures we want to measure. The large variations are highly undesirable but unavoidable. In order to obtain reliable absorption coefficient data it is necessary to maintain the entire system in a very stable condition. In spite of the variable reflectivity RAP is the best available crystal for the task. Other acid phthalates and clinochlore have worse variations or worse resolution or both. RAP suppresses all higher-order reflections by at least a factor of 20 over the range of measurement and has resolving power equivalent to KAP.[19] It should be noted that although coated gratings should have much less of this problem, the effect may not be ignored. This was recognized from the outset of such measurements.[20]

The spectrometer has been previously described.[21] It has now been automated by means of stepper motors, a Canberra 1740 Bragg beam scan control modified for operation of two motors independently or together, and a Canberra 8100 multichannel analyzer modified for interaction with a TI700 computer terminal. This approach permits all data to be processed by the computer, read in and out of the analyzer, and eventually stored on small magnetic tape cassettes.

Wavelengths (energies) have been determined from the measured Bragg angles, corrected for zero error and dispersion in the crystal. Shifts and broadening of linelike features due to instrument misalignment and beam divergence are less than 4×10^{-3} Å (0.1 eV). The absorption coefficient measurements were all made with an RAP crystal analyzer whose resolution width varies over the range of interest from about 0.03 to 0.02 Å (0.75 to 0.5 eV). Absorption spectra have not been corrected for effects of the instrument window function because it is not accurately known in this region. Energies in eV were obtained from the relation $E = hc/\lambda = hc/2d\sin\theta = 475.367/\sin\theta$ with an uncertainly of ±0.3 eV due primarily to the uncertainty in correction for dispersion in the crystal. Some fine details at small amplitude have undoubtedly been lost in the poor statistics and poor resolution of the measurements.

Scans were made with filters in and out of the beam to get absorption coefficients from the ratio $[\ln(I_0/I)/\rho x] = \mu/\rho$, where μ/ρ is the desired mass absorption coefficient and ρx is the measured surface density of the gas.

This is far from an optimum approach to absorption coefficient measurements because of the strong energy-dependent variation in properties of the analyzer crystal. Absorption coefficient measurements with similar structure near threshold were made three years ago on Parlodion using a KAP crystal. These data agreed with the ones measured this year using an RAP crystal, thus confirming at least the reproducibility with this technique. Although the approach is not optimum, it has provided the first quantitative data on absorption structure around the oxygen K edge in molecular gases CO and N_2O, and additional improved results on O_2 and CO_2.

Measurements were made of the reference spectrum before and after the filtered spectrum and the average reference spectrum was used for the determination of transmission. No feature in the two reference spectra ever differed by more than 2%; the contamination O $K\alpha$ line usually increased by 1% to 2% over the measurement period and this showed up in the measurements at low pressure as a small erroneous dip in μ/ρ at the O $K\alpha$ position. Counting rates in the unfiltered reference beam ranged from 500 to 2500 cps. The contamination background, which was measured as previously described and subtracted from both the reference and filtered beams independently, was 22 to 37 cps. The range 500 to 600 eV (52° to 70°) was covered with 450 data channels with usually 10-sec dwell per channel on the reference beam and 20-sec dwell per channel on the filtered beam. Shorter scans at higher resolution were made to bring out weak bumps, some of which are not evident in the data graphs shown in the Sec. III.

III. RESULTS

A. Data

Measured mass absorption coefficients are presented in Figs. 2–6 and Tables I–V. Each figure has an angle abscissa running linearly from 52° to 70°, which is 603.25 to 505.87 eV from the formula already given. The peaks identified in each graph are listed with their energies and other parameters in Table I. Binding energies are electron spectroscopy for chemical analysis (ESCA) values.[10,22] The curves in each figure are hand drawn through the point scatter on each data plot. The point scatter was on the average ±3% (1σ), except for the O_2 data below 520 eV where the scatter was ±7% (1σ).

Before discussing the spectrum of each gas, we need to comment on some general characteristics of the data. Foremost is the "thickness effect,"[18] whose large influence can be seen by comparing Figs. 2 and 3 for O_2. Data in Fig. 2 (shorter cell) were obtained at one-tenth the column density of Fig. 3. As the sample thickness or density is increased, the strong absorption peaks adjacent to the low absorption region (above 64°) are reduced in amplitude. This is not simply the smearing effect of a low resolution instrument, which is not dependent on the sample thickness. Rather this effect arises from the large difference in transmitted intensity across the photoabsorption transition region. When the instrument is located at the position of peak 1, the tail of the instrument window function extending far out into the high transmission region at higher angles (lower energies) collects counts which cause the apparent transmission to exceed the correct value. Far outside the 60° to 65° range in which the absorption is changing by large factors the measured absorption coefficients will be much less affected. Because of this phenomenon, the optimum absorber thickness ρx is much less than one would compute on the

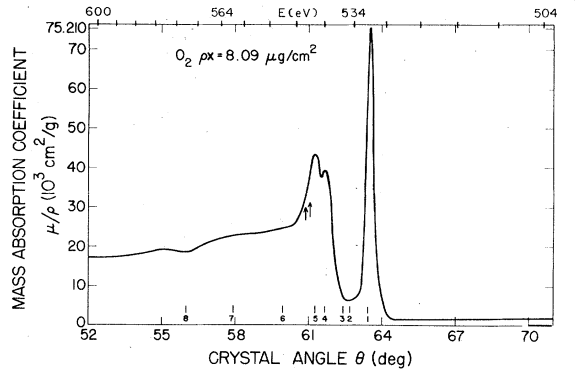

FIG. 2. Measured molecular oxygen mass absorption coefficient using the short cell to reduce the thickness effect (Ref. 18). The statistical precision was poor in this case. Consequently the hand-drawn average curve contains an exaggerated peak around 55.5° that was barely detectable and closer to 56° in the more precise data with the larger cell (Fig. 3). However, the shapes and amplitudes of the three large peaks are better revealed in these low ρx data. The ESCA binding energies are marked by arrows. Vertical lines mark the peak positions determined from subsequent scans with better statistics. The energy scale, marked in 6-eV intervals at the top, is nonlinear.

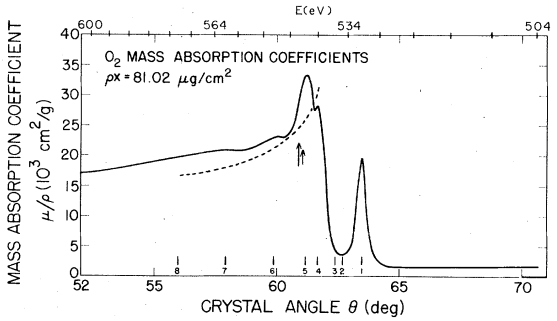

FIG. 3. Measured molecular oxygen mass absorption coefficient using the long cell. Here the large peaks are suppressed from their true values by the thickness effect (Ref. 18), but the values above 65° and below 60° are reliably determined. Some very weak bumps do not appear in this plot, which was hand sketched through the point scatter from a single data run. The ESCA binding energies are marked by arrows. Vertical lines mark the peaks discussed in the text. Calculations by Gerwer and McKoy (Ref. 27) are shown by the dashed line. The energy scale, marked in 6-eV intervals at the top, is nonlinear.

TABLE I. Parameters of peaks in photoabsorption spectra of O_2, CO_2, CO, and N_2O.

Gas	Peak no.	Peak energy[a] (eV)	Peak μ/ρ (cm^2/g)	ρx ($\mu g/cm^2$)	P/V ratio[b]	Extrapolated peak μ/ρ[c] (cm^2/g)	Extrapolated P/V ratio[c]	Peak width[d] (eV)
O_2	1	530.9	75 000	8.09	47.0	105 000	65.6	1.5
			19 200	81.65	12.8	•••	•••	•••
			19 400	81.02	13.0	•••	•••	•••
	2	535.0	•••	81.65	•••	•••	•••	Barely detectable discrete feature
	3	535.9	•••	81.65	•••	•••	•••	Barely detectable discrete feature
	4	539.9	39 250	8.09	24.1	40 000	24.5	1.8 approximate; 4 and 5 blended
			27 800	81.65	17.1	•••	•••	•••
			28 000	81.02	17.2	•••	•••	•••
	5	542.0	43 200	8.09	26.5	44 000	27.0	2.6 approximate; peak is just below
			32 800	81.65	20.1	•••	•••	the 1s binding energy
			33 300	81.02	20.4	•••	•••	
	6	548.9	23 200	81.65	•••	•••	•••	Broad and weak
			23 100	81.02	•••	•••	•••	
	7	560.5	21 200	81.65	•••	•••	•••	Broad and weak
			21 000	81.02	•••	•••	•••	
	8	572.4	19 700	81.02	•••	•••	•••	Broad and barely detectable
CO_2	1,2	535.3	62 000	11.10	14.2	66 600	15.2	2.0; could be a barely resolved
			59 000	11.44	13.5	63 400	14.5	doublet of nearly equal
			19 100	108.69	4.4	•••	•••	intensities?[e]
			19 000	109.39	4.4	•••	•••	
			19 100	112.60	4.4	•••	•••	
	3	539.1	20 000	11.44	•••	22 000	•••	Discrete but weak and blended to 4
	4	541.9	18 300	109.39	•••	21 000	•••	2.6 approximate; peak is just above
			18 700	112.60	•••	21 000	•••	the 1s binding energy
	5	548.2	17 300	109.39	•••	•••	•••	Very weak
	6	552.0	19 000	109.39	•••	•••	•••	Very weak peak on the side of 7
	7	554.0	21 600	109.39	•••	•••	•••	2.0 approximate; blended to 8
			21 800	112.60	•••	•••	•••	
	8	558.7	23 600	109.39	•••	•••	•••	6.5; broad and strong
			23 750	112.60	•••	•••	•••	
	9	578.5	17 150	112.60	•••	•••	•••	Very weak and broad
CO	1	531.2	14 000	7.20	2.3	15 000	2.5	1.6 approximate; weak feature obscured on some scans by variations in OK_α on source
	2	534.2	61 000	7.20	9.0	69 000	10.2	1.6
			24 600	71.02	3.6	•••	•••	
			24 400	72.03	3.6	•••	•••	

TABLE I (*Continued*).

Gas	Peak no.	Peak energy[a] (eV)	Peak μ/ρ (cm^2/g)	ρx ($\mu g/cm^2$)	P/V ratio[b]	Extrapolated peak μ/ρ[c] (cm^2/g)	Extrapolated P/V ratio[c]	Peak width[d] (eV)
	3	539.1	9 600	71.02	•••	•••	•••	Discrete and barely detectable
			8 600	72.03	•••	•••	•••	
	4	540.4	10 400	71.02	•••	•••	•••	Discrete and barely detectable
	5	541.7	12 800	71.02	•••	•••	•••	Edge of oxygen 1*s* binding energy
	6	550.6	24 500	71.02	•••	27 000	•••	3 approximate; board and strong
			23 900	72.03	•••	27 000	•••	above 1*s* binding energy
	7	569.1	17 700	71.02	•••	•••	•••	Broad and very weak
N_2O	1	535.0	23 200	110.15[f]	2.0	72 000[g]	6[g]	2.1 approximate; blend with 2
	2	536.7	21 000	110.15	1.8	•••	•••	Equal or less than peak 1
	3	539.6	22 500	110.15	1.9	•••	•••	3 approximate; blend with 4
	4	541.5	20 400	110.15	•••	•••	•••	Weak bump on side of 3
	5	547.8	18 000	110.15	•••	•••	•••	Very weak
	6	552.2	19 250	110.15	•••	•••	•••	Broad
	7	575.1	16 500	110.15	•••	•••	•••	Very weak

[a] Accuracy of peak energy is ±0.3 eV for strong peaks; ±1 eV for weak peaks.

[b] P/V is the ratio of peak μ/ρ to the value of μ/ρ in the valley on the low-energy end of the spectrum around 522 eV.

[c] Extrapolated peak μ/ρ and P/V ratio are estimated from a linear fit to measurements at two pressures; accuracy is probably better than ± 20% except for N_2O.

[d] Peak widths have not been corrected for instrument width. The latter is about 1 eV but its exact shape is not known in this region.

[e] The dominant CO_2 peak appeared double in two of our high-dispersion spectra and single in a third.

[f] The average of two runs at 110.02 and 110.30 which gave very close agreement.

[g] The extrapolated values are very approximate for N_2O because we did not get a low ρx scan for this gas; we approximated the curve slope to get these extrapolated values.

TABLE II. Mass absorption coefficients[a] for oxygen in the range 500–600 eV.

E (eV)	μ/ρ (cm^2/g)	E (eV)	μ/ρ (cm^2/g)	E (eV)	μ/ρ (cm^2/g)
506	1 690	555	21 300	571	20 100
510	1 680	556	21 150	572	20 050
513	1 670	557	21 050	573	19 950
516	1 650	558	20 950	574	19 850
519	1 630	559	21 000	575	19 700
522	1 620	560	21 150	576	19 550
525	1 605	561	21 100	577	19 450
546	24 100	562	21 000	578	19 300
547	23 200	563	20 900	579	19 200
548	23 000	564	20 700	582	18 800
549	23 100	565	20 600	585	18 600
550	22 900	566	20 500	588	18 350
551	22 600	567	20 350	591	18 100
552	22 300	568	20 300	594	17 900
553	22 000	569	20 250	597	17 600
554	21 600	570	20 200	600	17 300

[a] Values of mass absorption coefficient μ/ρ are listed for molecular oxygen. To convert to molecular oxygen cross sections in Mb multiply by 5.3138×10^{-5}. Profiles of the strong peaks are not tabulated because they are made much too small in the data by the thickness effect. See Table I for extrapolated peak values.

basis of counting statistics and background. In fact, the optimum thickness would be zero. Obviously as the gas thickness or density is reduced the difference in transmission between the filtered and unfiltered beams becomes smaller and the accuracy of the μ/ρ determination rapidly deteriorates. Therefore, only the strong absorption peaks in Fig. 2 have reasonable statistical reliability and the entire spectrum could be too high by about 10% due to the cell length uncertainty. We included these data to illustrate the thickness effect and our correction procedure for removing it and estimating the true peak heights.

Figures 3–6 show results for scans using the large cell. All these plots will have the strong absorption peaks suppressed from their true values but the regions above and below the strong peaks are reliably determined. In these low- and high-energy ranges the statistical precision is everywhere within ±3% (1σ), except for O_2 in the low-energy region where it is ±7% (1σ).

In order to get correct absorption coefficients on the strong peaks, we made measurements at high and low values of ρx and then used a two-point linear fit to μ/ρ vs ρx and extrapolated this line to zero for all but the strongest peak. More values of ρx were used on the strongest peak and a nonlinear curve was fitted and extrapolated to zero ρx. This procedure was applied only to the peak values, not to the entire absorption profiles. The measured and extrapolated values of μ/ρ, peak to valley ratios, and peak widths are given in Table I with the peak energies. The extrapolated peak values could be biased as much as 10% too high. Our intention in this table is simply to illustrate the approximate magnitude of the peaks relative to the photoionization continuum. The large and small peaks will be discussed below. Some very small peaks in Table I are not evident in the figures. At the present state of comparison between theory and experiment we do not attach much significance to any peaks unless they are obvious in Figs. 3–6.

TABLE III. Mass absorption coefficients[a] for carbon dioxide in the range 500–600 eV.

E (eV)	μ/ρ (cm^2/g)	E (eV)	μ/ρ (cm^2/g)	E (eV)	μ/ρ (cm^2/g)	E (eV)	μ/ρ (cm^2/g)
506	4 780	543	18 150	558	23 600	573	17 500
510	4 680	544	17 600	559	23 650	574	17 450
513	4 620	545	17 300	560	23 400	575	17 450
516	4 550	546	17 150	561	22 800	576	17 400
519	4 480	547	17 200	562	22 100	577	17 350
522	4 420	548	17 250	563	21 300	578	17 250
525	4 370	549	17 150	564	20 500	579	17 100
528	4 400	550	17 150	565	19 800	582	16 700
531	4 500	551	17 500	566	19 150	585	16 200
532	4 750	552	19 050	567	18 750	588	15 900
538	9 800	553	20 600	568	18 400	591	15 600
539	14 500	554	21 550	569	18 100	594	15 400
539.5	15 900	555	21 300	570	17 900	597	15 200
540	16 350	556	22 000	571	17 700	600	15 100
541	17 950	557	22 950	572	17 600	603	15 000
542	18 300						

[a] Values of mass absorption coefficient μ/ρ are listed for molecular carbon dioxide. To convert to molecular cross sections in Mb multiply by 7.3084×10^{-5}.

TABLE IV. Mass absorption coefficients[a] for carbon monoxide in the range 500–600 eV.

E (eV)	μ/ρ (cm^2/g)	E (eV)	μ/ρ (cm^2/g)	E (eV)	μ/ρ (cm^2/g)	E (eV)	μ/ρ (cm^2/g)
506	6 930	542	12 750	557	19 000	572	16 650
510	6 810	543	13 750	558	18 650	573	16 400
513	6 720	544	14 650	559	18 350	576	16 000
516	6 635	545	15 800	560	18 100	579	15 600
519	6 550	546	17 200	561	17 950	582	15 350
522	6 460	547	18 450	562	17 850	585	15 100
525	6 375	548	20 000	563	17 750	588	14 800
528	6 650	549	22 050	564	17 650	591	14 450
531	7 250	550	23 800	565	17 550	594	14 150
532	7 700	551	23 800	566	17 500	597	13 980
537	8 450	552	22 550	567	17 400	600	13 730
538	7 800	553	21 150	568	17 300	603	13 540
539	8 600	554	20 500	569	17 170		
540	9 650	555	20 000	570	17 020		
541	11 300	556	19 400	571	16 860		

[a] Values of mass absorption coefficient μ/ρ are listed for molecular carbon monoxide. To convert to molecular cross sections in Mb multiply by 4.651×10^{-5}.

For the high- and low-energy ranges where no strong peaks occur we have listed numerical values of the absorption coefficients in Table II. This tabulation will allow reconstruction of μ/ρ vs energy to the accuracy of the original data, except that some small peaks may still be missed due to their weakness and the coarseness of the grid. While these peaks are useful to qualitative understanding of the absorption spectra they are not essential to the quantitative tabulation and it would be premature to examine them in more quantitative detail.

TABLE V. Mass absorption coefficients[a] for nitrous oxide in the range 500–600 eV.

E (eV)	μ/ρ (cm^2/g)	E (eV)	μ/ρ (cm^2/g)	E (eV)	μ/ρ (cm^2/g)
506	12 650	546	17 850	576	16 400
510	12 450	547	17 950	579	16 050
513	12 330	548	18 050	582	15 700
516	12 050	549	18 200	585	15 450
519	11 950	550	18 300	588	15 200
522	11 900	551	18 700	591	14 900
525	11 820	552	19 120	594	14 700
528	11 750	553	19 250	597	14 500
531	11 800	555	19 200	600	14 300
541	20 050	558	20 050	603	14 100
542	19 600	561	18 400		
543	18 500	564	17 820		
544	18 020	567	17 200		
545	17 900	570	16 800		
		573	16 600		

[a] Values of mass absorption coefficient μ/ρ are listed for molecular nitrous oxide. To convert to molecular cross sections in Mb multiply by 7.3092×10^{-5}.

B. Comparison to other data

There are three comparison sets of measured data. LaVilla[2] has used a technique basically the same as that employed by us to study O_2 and CO_2. Bodeur, Senemaud, and Bonnelle[23] measured μ/ρ for O_2 with a curved crystal spectrometer. Henke and Elgin[24] made measurements at discrete wavelengths on O_2 and then made a compilation of available data on all the light elements.

We will compare first to LaVilla who presented his results in the form of a graph of the cross sections versus energy. We have shifted his energy scale about 1 eV to make the strongest absorption peak coincide with our spectra. Then we scaled the cross sections from his graph at selected points. Because of the thickness effect and nonidentical experimental conditions, we do not expect agreement between the two data sets on the strong peaks. Also, the energy region below the K edge is extremely difficult to determine reliably at the low pressure used by LaVilla. However, in the high-energy range of overlap the two sets of measurements may be compared. After converting LaVilla's cross sections from atomic to molecular, we find our values about 1.5 times as large as LaVilla's. This is reasonable agreement in view of the difficult conditions under which LaVilla's measurements were made.

Fortunately we were able to benefit from his experience when our measurements were made the second time around. Comparison to Bodeur *et al.*[23]

was also made by scaling their curves for O_2. Our peaks 1, 4, and 5 agree very well qualitatively with their peaks 1, 2, and 3. Above 545 eV we find features that probably correspond to their dashed curve qualitatively. For quantitative comparison we have scaled their solid curve and find our data 1.25 times larger from 550 to 570 eV. Based on their brief description of their experiment we believe this agreement is reasonable.

Thirdly we may compare to Henke and Elgin.[24] Here the agreement is very good and it becomes necessary to discuss what order of agreement can be expected. It has been the custom in x-ray physics to treat absorption coefficients as atomic properties independent of the compound or physical state. Indeed this was the reason for introducing the mass absorption coefficient instead of the cross section. For absorption by low-Z elements at low energies the presence of atomic neighbors has a pronounced effect on the absorption cross sections near the photoionization threshold, as is evident from our data and numerous earlier examples.[4-16] The presence of strong bound-state excitations and strong resonances in the continuum, both of which depend in detail on atom interactions at the molecular level, preclude the possibility of deducing atomic cross sections that apply to all states of atomic aggregation. However, oscillator strength must be conserved. If one integrates the oscillator strength in these features, the deviations from atomic properties do not appear so great. A strong Rydberg series of bound-state absorption would occur in atomic oxygen anyway. Also the integrated continuum resonances above the binding energies are only a small fraction of the total photoionization cross section integrated over all energies. Thus the effect of molecular interactions, in particular potential barriers, is to redistribute oscillator strength. Only a small fraction of the total available oscillator strength is required to explain the localized resonances. Therefore, we may expect that at high and low energies, relative to the region of large variations near threshold, the cross sections derived from molecular or solid-state measurements will approach the purely atomic cross sections. For example, simple power-law integration of data such as in Figs. 3–6 shows the oscillator strength in the peaklike features above the K-edge is only about 1% of the total continuum oscillator strength. Since these features in our data on all four gases have disappeared or become very small by 600 eV, we should expect our measured data to approach the tabulations of Henke and Elgin within a few percent. The same should be true at low energies, less than 530 eV, except that oxygen does not contribute much absorption on the low-energy side and statistical uncertainties could be comparable to the signal to be derived.

Table VI shows confirmation of the above expectation. At 600 eV the largest difference is 1%. CO_2 and N_2O are within 3% at both high and low energies. O_2 is higher in our data by about 10% at low energies where our precision is lowest. Overall the agreement is everywhere well within the combined accuracy expected for the two sets of data.

Further confirmation is available by comparison of atomic cross sections derived from molecular measurements. Henke and Elgin[24] list measurements of absorption coefficients at discrete line energies for O_2. Their measurements have a precision of about 0.1%. At energies below and well above the ionization edge the oxygen atomic cross section should be one-half the molecular cross section. By the same reasoning if one goes far from the K edge of oxygen in CO_2 the atomic oxygen cross section should be given by $\sigma[0]=\frac{1}{2}\{\sigma[CO_2]-\sigma[C]\}$, where $\sigma[CO_2]$ has been measured in this work and $\sigma[C]$ should be accurately given by the tables in Henke and Elgin because the energies are far above the carbon K edge. Table VII shows that

TABLE VI. Comparison of measured mass absorption coefficients.

	O_2[a]			CO_2			CO			N_2O		
E (eV)	Henke & Elgin	LASL[b]	Ratio	Henke & Elgin	LASL	Ratio	Henke & Elgin	LASL	Ratio	Henke & Elgin	LASL	Ratio
600	17 360	17 300	0.997	15 000	15 100	1.007	13 650	13 730	1.006	14 150	14 300	1.011
525[b]	1 440	1 605	1.115	4 374	4 370	0.999	6 050	6 375	1.054	11 460	11 820	1.031
506	1 568	1 692	1.079	4 791	4 780	0.998	6 633	6 930	1.045	12 564	12 650	1.007

[a] The Henke and Elgin values for O_2 were measured at discrete wavelengths. We fit a curve to their measurements to get values at 600 and 506 eV; one of their discrete energies was $OK\alpha$ at 525 eV. For the other gases the μ/ρ values are obtained from their semiempirical tables.

[b] Los Alamos Scientific Laboratory (LASL) values at 525 eV were subject to small variations in a weak $OK\alpha$ contamination line from the gold anode. The trend of data in this table indicates that errors from this cause were not significant.

TABLE VII. Atomic cross sections derived from molecular data around the ionization threshold.

E (eV)	LASL $\sigma[CO_2]$ (Mb)	HE [a] σ[C] (Mb)	Derived [b] $\sigma[O]=\frac{1}{2}\{\sigma[CO_2]-\sigma[C]\}$ (Mb)	LASL [c] σ[O] (Mb)	H [d] σ[O] (Mb)	Derived σ[O] / $H\sigma$[O]	LASL σ[O] / $H\sigma$[O]
506	0.349	0.267	0.0410	0.0449	0.0417	0.98	1.08
510	0.342	0.262	0.0402	0.0446	0.0409	0.98	1.09
513	0.338	0.258	0.0402	0.0444	0.0404	1.00	1.10
516	0.332	0.254	0.0390	0.0438	0.0398	0.98	1.10
519	0.327	0.250	0.0384	0.0433	0.0393	1.00	1.10
522	0.323	0.247	0.0382	0.0430	0.0388	0.98	1.11
525	0.319	0.243	0.0380	0.0426	0.0383	0.99	1.11
531	0.329	0.236	0.0464	2.126	0.636	0.07	3.34
535.3	4.750	0.232	2.26	0.100	0.622	3.63	0.16
540	1.195	0.226	0.484	1.063	0.608	0.80	1.75
560	1.710	0.206	0.752	0.561	0.553	1.36	1.01
580	1.240	0.189	0.526	0.507	0.504	1.04	1.01
600	1.104	0.174	0.465	0.460	0.461	1.01	1.00

[a] Reference 24.

[b] Carbon cross section assumed to be the atomic value because the energy E is far above the carbon K photoabsorption threshold.

[c] Measured molecular cross section (Table II) divided by 2.

[d] Cross section for molecular oxygen from Ref. 24 and divided by 2. Henke's measured data were used and a curve was fit to his points to get values at energies in this table.

below the K edge our derived values of σ[O] from CO_2 data are virtually identical to the Henke and Elgin results while our measured σ[O] from O_2 are consistently higher by about 10%. This is within the combined accuracy of our measurements and the curves fit to the discrete data of Henke and Elgin in the low-energy region. It is by chance that the cross sections derived from CO_2 are within 2% of the tabulated data. Above the K edge, where our accuracy is better, the agreement is within 1% between our measured and derived values, and between this work and Henke and Elgin.[24] The same analysis applied to our CO data at 600 eV gave an atomic oxygen cross section in agreement with the tabulations within 1%; and σ[O] from N_2O agreed within 2%. On the low-energy side the σ[O] contribution is so small in these two gases that nothing can be decided. We conclude that below the binding energy and at some 5 Ry or more above it the tabulations of atomic mass absorption coefficients should be reliable to a few percent for general application to atoms in any state of aggregation.

C. Comparison to theoretical data

Most calculations have been done for the continuous absorption outside the narrow region of structure. McGuire[25] has calculated the atomic photoionization cross sections for the elements. A curve fit to McGuire's calculations for oxygen shows the calculated values 15% below our measured values at 600 eV. The difference increases toward lower energies because of the molecular effects in the measured data near threshold. Veigele's[26] calculated value at 600 eV falls 8% below our measured value. This agreement is compatible with expectation. More detailed calculations have been done for oxygen by Gerwer and McKoy.[27] Above 545 eV our measured data never exceed their oxygen values by more than 20%, as shown in Fig. 3. The two curves approach coincidence at 547 eV.

Padial *et al.*[28] have carried out molecular orbital calculations on CO which may be compared with our absorption measurements above the oxygen K edge. Since resonance behavior was included in this work of Padial *et al.*, we shall defer the discussion to Sec. IV. These calculations were similar to those of Rescigno and Langhoff[29] which gave the best agreement with measurements on nitrogen.[12]

IV. DISCUSSION

All these gases show three common features: (i) resonance absorption to bound-state, unfilled molecular orbitals below the binding energy; (ii) resonances in the continuum at or above the binding energy that are explainable in terms of potential barrier effects; (iii) weak, broad features

in the continuum that may arise from shake-up of valence electrons and possibly in some cases from the one-electron spectrum peculiar to the molecular environment. In addition one can just discern some weak Rydberg transitions in all but N_2O. It seems probable that their absence in N_2O is caused by the low resolution and sensitivity of our measurements.

The main contributions of the present work have been the reasonably accurate quantitative results and sufficient sensitivity to permit the observation of some weak features not previously reported. We discuss below the qualitative aspects and some revised interpretations of the spectra made possible by these quantitative data.

A. Oxygen

Peaks that we have labeled 1–5 in Table I were observed by Nakamura *et al.*[5] and labeled *A*–*E*. (Peaks 2, 3, and 8 are not evident in Figs. 2 and 3. They were found on separate scans.) They identified the strongest peak 1 as a transition from the ground state of O_2 to the first permitted unfilled molecular orbital, $(2p\pi_g)^3\Pi$, and the remaining peaks as transitions to Rydberg states. Wight and Brion[9] observed the electron scattering equivalent of peaks 1, 4, and 5. They agreed with Nakamura *et al.*[5] on the assignment of peaks. LaVilla's[2] data show peak 1, plus peaks 4 and 5 merged into a single broad peak. Table VIII summarized the available data. From the location of peaks 4 and 5 below the binding energy (543.1 and 544.2), we agree that a Rydberg excitation is likely, but the large magnitude of the absorption and large breadth (see Fig. 2 and Table I) suggest there is a large admixture of oscillator strength caused by a potential barrier.[16] The magnitudes and locations of these peaks near threshold are readily understood as inner well discrete states in Dehmer's[15] description of potential barrier effects. A shape resonance is responsible for the strength of the features below the ionization threshold, such as peak 1 in this gas.

Peaks 6–8 are all weak and broad (as nearly as one can tell from features that stand only a few percent above the trend line). There are three apparent explanations of these weak bumps in the photoionization continuum: (a) The molecular equivalent of extended x-ray absorption fine structure (EXAFS) seen in solids; (b) double excitation; and (c) simultaneous excitation and ionization (shake-up).

The molecular equivalent of EXAFS is a diffraction effect in molecules as it is in solids, arising from multiple scattering of the outgoing electron waves. Dehmer and Dill[16] have shown for N_2 that the higher angular momentum waves ($l = 2, 3$, etc) mixed into the final state by the anisotropic molecular field cause oscillations in the partial photoionization cross sections at energies more than a few rydbergs above the ionization threshold. However, much of this oscillatory behavior from different waves cancels with the result that the molecular EXAFS is expected to be <1% of the total cross section. This is verified in N_2 by Bianconi *et al.*[12] However, in O_2 the centrifugal barrier effects are pushed back to the threshold region and we cannot rule out very weak (1%) EXAFS in the range 1–5Ry.

Double excitation here means excitation of the 1*s* electron, most probably to the bound $2p\pi_g$ orbital configuration, and simultaneous excitation of a valence 2*s* or 2*p* electron to a higher *nl* state. This process was observed by Schnopper[30] in argon where the *KM* double excitation was about 8% of the total cross section. Wuilleumier[31] observed the *KL* double excitation in neon at 2% and the *LN* double excitation in krypton at about (4–7)% (there were four observed peaks). In each case the ionization continuum for the outer electron was also observed, corresponding to excitation plus ionization (shake-up). Thus, there is ample evidence that double excitation can explain features in the continuum at the few percent level. We note that double excitation is not observable in x-ray photoelectron spectroscopy (XPES) with discrete line x-ray excitation because energy would not be conserved.

Shake-up in our context can be either the excitation $1s \rightarrow 2p\pi_g$ simultaneous with ionization of an outer shell 2*s* or 2*p* electron or ionization $1s \rightarrow \infty$ simultaneous with excitation of a valence 2*s* or 2*p* electron. Thus shake-up can appear in x-ray photoabsorption spectroscopy (XPAS) in two modes: (i) as a continuum following a discrete double excitation line, or line series, and (ii) as a continuum rise superposed upon the single-electron ionization continuum as the incident x-ray energy increases past the threshold for inner-shell ionization plus outer-shell excitation. In either case the limited resolution and sensitivity of our XPAS system will lead to a bump on the continuum, probably with little discernible structure. In XPES data, however, shake-up appears as discrete features above the discrete peak binding energy associated with ionization by removal of a single core electron. These XPES peaks will lie at the low-energy threshold of XPAS continuum bumps in mode 2 above. In mode 1 the XPES peaks will lie between the XPAS double excitation line series and the associated continuum. In high resolution XPES data the discrete shake-up peaks are followed by the continuum due to double ionization or shake-off. Double ionization is not observable in

TABLE VIII. Comparison of spectral features from several different measurements. (a) O_2 binding energy 543.1 eV; 61.08° and 544.2 eV; 60.87°. (b) CO_2 binding energy 541.1 eV; 61.46°. (c) CO binding energy 542.6 eV; 61.17°. (d) N_2O binding energy 541.2 eV; 61.445°.

(a)

	This work		Ref. 5		Ref. 9		Ref. 2	
Peak no.	*E* (eV)	Width (eV)	*E* (eV)	Width (eV)	*E* (eV)	Width (eV)	*E* (eV)	Width (eV)
1	530.9	1.5	532	≈1.5	530.8	1.0	532	≈2
2	534.9	Narrow	534.8	Narrow	•••	•••	•••	•••
3	535.9	Narrow	536.8	Narrow	•••	•••	•••	•••
4	539.9	≈1.8	540	≈2	539.2	≈1.7	•••	•••
5	541.9	≈2.6	542	≈3	541.9	≈2.5	543	≈4
6	548.9	Broad	548[a]	•••	•••	•••	•••	•••
7	560.5	Broad	•••	•••	•••	•••	•••	•••
8	572.4	Broad	•••	•••	•••	•••	•••	•••

(b)

	This work		Ref. 9		Ref. 2	
Peak no.	*E* (eV)	Width (eV)	*E* (eV)	Width (eV)	*E* (eV)	Width (eV)
1,2	535.3	2.0	535.4	1.4	535.4	•••
3	539.1	Narrow	538.7	≈1.0	•••	•••
4	541.9	≈2.6	541.5[b]	≈3	•••	•••
5	548.2	•••	548[a]	•••	•••	•••
6	552.0	•••	•••	•••	•••	•••
7	554.0	≈2	553	≈3	•••	•••
8	558.7	≈6.5	558	≈6	•••	•••
9	578.5	Broad	•••	•••	•••	•••

(c)

	This work		Ref. 5		Ref. 8	
Peak no.	*E* (eV)	Width (eV)	*E* (eV)	Width (eV)	*E* (eV)	Width (eV)
1	531.2	≈1.6	529	≈1.2	•••	•••
2	534.2	1.6	532	•••	534.0	1.3
3	539.1	Narrow	536	≈0.5	538.8	1.0
4	540.4	Narrow	537	≈0.5	539.8	1.0
5	541.7	•••	538[c]	≈0.5	540.9	1.0
6	550.6	≈3	•••	•••	550	Broad
7	569.1	Broad	•••	•••	•••	•••

(d)

	This work		Ref. 9	
Peak no.	*E* (eV)	Width (eV)	*E* (eV)	Width (eV)
1	535.1[d]	~2.1[d]	534.6	1.2
2	536.7	<2.1[d]	536.5	≈1.0
3	539.6	≈3[d]	538.8	≈1.0
4	541.5[e]	•••	540.0	•••
5	547.8	•••	•••	•••
6	552.2	Broad	552	Broad
7	575.1	Broad	•••	•••

[a] Not listed in the reference work, but a small bump corresponds to ours.

[b] This peak listed by Wight and Brion apparently is meant to be a weak Rydberg transition at the leading edge of the peak we call 4. The peak position and width listed here were scaled from their graph.

[c] Nakamura *et al.* (Ref. 5) see a series of weak, narrow peaks starting at the binding energy and running to 2 eV or more higher. These would be Dehmer's (Ref. 15) inner-well discrete states.

[d] Peak positions in this case are influenced by the thickness effect and peak widths are too large for the same reason. We did not get a low-density run on this gas.

[e] Peak is probably a blend of a line with the *K*-ionization jump.

XPAS data because Carlson *et al.*[32] showed that its cross section disappears at threshold excitation photon energy. However, shake-up is finite or a maximum at threshold.[30,31,33,34] The problem of interpreting shake-up here is that we observe at threshold excitation and the relevant XPES observations have been made far above threshold. The shake-up peaks observed in XPES[35] with Al $K\alpha$ excitation might not be the features one would observe at threshold excitation in our XPAS data because the parent partial photoionization cross sections (and by inference the shake-up cross sections) generally have quite different variation with energy.[36,37] The two techniques could be made equivalent by using threshold excitation in XPES by means of monochromated synchrotron radiation, but this has not yet been done for inner-shell absorption.

Carlson *et al.*[35] observed oxygen shake-up peaks with Al $K\alpha$ excitation energy at 10 eV (10%–15% of total photoionization cross section) and at 22 eV (5%–7%) above the lower binding energy. Since these peaks are several eV above our peaks 6 and 7, we conclude that shake-up can explain our observed peaks 6–8 if (a) a different set of peaks with different nl is contributing in our threshold excitation observations, or (b) the double excitation mode 1 above is dominant in the shake-up process in oxygen.

This conclusion is strengthened by comparison to the nitrogen K-edge data in N_2 and N_2O. Biaconi *et al.*[12] and Wight and Brion[9] attribute the peak F in the data on N_2 and N_2O (Ref. 12) to double excitation transitions. They concentrate on matching the stronger peak G to the model of Dehmer and Dill,[16] who also attribute peak F to double excitation. The well-resolved shake-up peaks in the data of Gelius[38] are compatible with this assignment because the double excitation peak F is unobservable in XPES and the observed peaks could be merged with the relatively large peak G. However, peak G can be adequately explained as a potential barrier resonance. Thus, shake-up contributions to N_2 and O_2 photoabsorption data seem to be small. A similar situation will be seen to exist in the data on CO_2 and CO. It will require better resolving power and much greater sensitivity measurements to sort out the relative contributions of these three explanations of weak bumps 6–8. Shake-up and double excitation seem to be the most likely explanations.

Our interpretation of the oxygen absorption structure is that the potential barrier effect causes an increase of oscillator strength near the photoionization threshold at the expense of higher energies. Therefore, we expect better agreement with Gerwer and McKoy[27] (see Fig. 3) after all the resonance channels and multiple-electron transitions have been included in the calculations.

B. Carbon dioxide

All the CO_2 peaks except 6 and 9 in our designation were seen in electron scattering spectra by Wight and Brion.[9] LaVilla[2] resolved the strongest peak 1, 2. (Peaks 5 and 6 are not evident in Fig. 4.) Again the dominant peak 1, 2 comes from excitation of an oxygen 1s electron to a bound-state molecular orbital $2\pi_u$. The peak is broad enough to contain two orbitals and their unresolved vibrational structure. Some of our scans hinted of a barely resolved doublet, which would be the orbital splitting.[9] Some scans also showed a very weak feature at about 530.7 eV, but the slight variability of the nearby O $K\alpha$ contamination line precluded a definite detection. Peak 3 is probably an additional Rydberg transition $3p\sigma_u$. Peak 4 can be understood as an inner-shell quasidiscrete state just above the binding energy.[15]

Our quantitative photoionization data make possible a revised explanation of the remaining features. We suggest that weak features 5, 6, and 9 and a fraction of peaks 7 and 8 are groups of shake-up transitions, and that peaks 7 and 8 owe most of their intensity to potential barrier effects. Wight and Brion[9] explained all of peaks 7 and 8 as double excitation and shake-up transitions because these were the only interpretations known at that time. The energies are right, but the intensities are wrong for this interpretation. Allan *et al.*[10] indeed measured a group of XPES shake-up satellites from CO_2 with energies corresponding to the range of our peaks 6–8. However, they were using Mg $K\alpha$ radiation and observed a maximum relative intensity of 5.8% for the strongest satellite. At the threshold photon energy associated with our measurements it is highly unlikely that the 37% relative intensity we see could arise from shake-up. It is much more

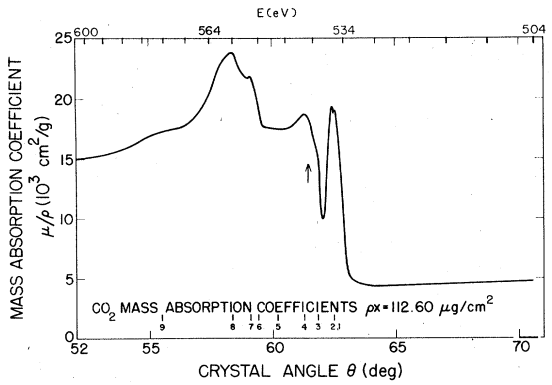

FIG. 4. Measured molecular carbon dioxide mass absorption coefficient using the long cell. See captions to Figs. 2 and 3 for more information.

probable that the weak shake-up transitions are overwhelmed in this range by a potential barrier peak, which in N_2 has been shown quantitatively to reach such large relative intensity by Dehmer and Dill.[16] On the other hand, the appearance of a very weak shake-up feature at 548 eV (peak 5), which was not evident in the electron spectra of Allan *et al.*,[10] can be explained as a feature lost in the noise of their data; it is also possible that we see a relatively stronger feature at this position because of the sensitivity of molecular-orbital transitions to energy of the exciting photons as shown by Wuilleumier and Krause[37] for neon, and by Gustafsson[39] for the valence orbitals of SF_6. Although the selection rules for shake-up transitions are different from one-electron transitions, the sensitivity to photon energy is a peculiarly molecular effect related to size and shape. Thus in the threshold region of photon energy the relative probabilities of various shake-up lines may differ from those observed at high photon energy.

Peak 9 was not included in the shake-up spectra presented by Allan *et al.*[10] or by Carlson *et al.*[35] It could have any of the three explanations mentioned earlier for weak bumps in the O_2 continuum. We have made no attempt to experimentally improve on the details of any of the supposed shake-up or double excitation features. The key to our interpretation is that they are always weak in these photoabsorption spectra and will require improved resolution and sensitivity for further analysis. The dominance of one-electron molecular transitions in peaks 7 and 8 is our point of emphasis.

C. Carbon monoxide

Seven peaks have been detected, of which peaks 1–5 were seen qualitatively with better resolution and sensitivity by Nakamura *et al.*[5] Wight *et al.*[8] observed peaks 2–6 in electron scattering. (Peak 4 is not evident in Fig. 5.) The energy scale of Nakamura *et al.*[5] needs to be shifted up a few eV to match the peaks, but there is no problem with identification. Although peak 1 was unambiguously seen and identified by Nakamura *et al.*,[5] its character in our data cannot be unambiguously defined because it is a weak forbidden transition that is sometimes obscured entirely in our data by small variations in the O $K\alpha$ source contamination line. Peak 2 is the always dominant excitation to a bound-state orbital, in this case the $2p\pi^*$ orbital and $^1\Pi$ state, and its breadth is attributed to excitation of several vibrational levels. In the references peaks 3–5 were clearly resolved, weak Rydberg transitions.

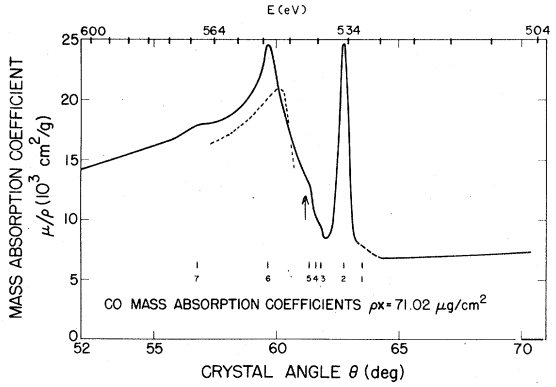

FIG. 5. Measured molecular carbon monoxide mass absorption coefficient using the long cell. A small peak was detectable at 531 eV, where the line is dashed, in some short cell scans. See captions to Figs. 2 and 3 for more information. The dashed line around peak 6 represents calculated results from Padial *et al.* (Ref. 28).

Again we offer a revised interpretation of the strong continuum resonance peak 6. This feature is about equal in relative intensity to the K-ionization cross section. Its tail extends out to ~600 eV and includes the weak bump 7. Carlson *et al.*[35] observed a shake-up peak with 8% relative intensity at 16 eV above the binding energy in CO along with weaker peaks at 8, 23, and 27 eV. Thus shake-up can explain our peaks only if the 8-eV peak grows two orders of magnitude as the excitation energy decreases from 1500 eV to threshold. This leads us to conclude that peak 6 is almost certainly not caused by electron shake-up, but is a potential barrier effect. The analogy with the Dehmer and Dill[16] calculation for N_2 is very close. Here any inner-well discrete states are minor except for peak 2.

This simple diatomic molecule provides an excellent test case for detailed molecular-orbital calculations, which have just been started by Padial *et al.*[28] They have done molecular-orbital calculations for the oxygen K-shell photoabsorption and obtain a shape resonance with its peak at 549 eV and a tail extending toward higher energies in very good agreement with our peak 6. In Fig. 5 we compare the calculated shape resonance to our peak 6. The agreements of peak position and shape are so close that improved measurements will be needed to refine the details in this region as the calculations continue to improve. We suggest the following approach to improved experimental photoabsorption cross sections. Crystal x-ray spectroscopy can provide good accuracy in the regions where structure is weak, around 500–520 eV and 560–600 eV. Electron scattering can provide good resolution and freedom from distortion in the region with large amplitude structure.[40,41] It follows that optimum measured results should come from electron scattering data that have been normalized to x-ray photoabsorption data at high

and low energies, say at 515 and 600 eV. A similar situation applies around the carbon K-edge and nitrogen K-edge, where crystal spectroscopy is feasible but suffers the same limitations. This procedure has been carried out by Kay *et al.*[41] with good results on the carbon and nitrogen edges. Their work on CO confirms the shape resonance interpretation of peak 6.

D. Nitrous oxide

Of the seven peaks detected in N_2O, peaks 4 and 5 are not evident in Fig. 5 because of their weakness. As in previous cases these were very weak bumps that did not come out of the statistical fluctuations on all scans. Peak 6 appears to be double humped in Fig. 6 and in one other scan at about the level of sensitivity of 1%.

Only one other relevant measurement of N_2O is known to us. Wight and Brion[9] observed our peaks 1–4 and 6 in electron scattering. Their technique is much better than crystal spectroscopy for locating and resolving peaks. For example, on peak 4 we were probably measuring a hump that blended their peak 4 and the K-ionization threshold jump. Their energy for peak 1 is probably more reliable also because we did not get a low-pressure scan on this gas and the thickness effect causes a peak displacement and considerable false broadening.

Assignment of the first four peaks in N_2O is rather risky without detailed calculations. All four transitions clearly involve excitation of an oxygen 1s electron to permitted molecular orbitals. They are discrete inner-well states. The effect of the potential barrier here appears mostly near the binding energy; it causes a large drop in oscillator strength just above the K-photoionization threshold, puts oscillator strength into the inner-well transitions, and possibly adds a little resonance in the continuum as part of peak 6. However,

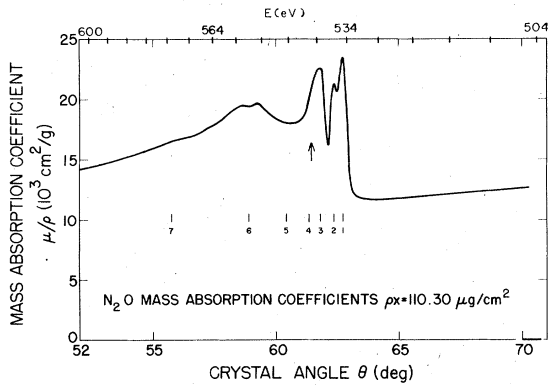

FIG. 6. Measured molecular nitrous oxide mass absorption coefficient using the long cell. See captions to Figs. 2 and 3 for more information.

the presence of a continuum resonance in this gas is not certain because shake-up states of the correct intensity and position to explain most of peaks 6 and 7 have been observed by Gelius[38] using Al $K\alpha$ excitation. Weak features 5 and 7 may arise as before from shake-up or they may be weak parts of the net molecular effect on single-electron partial photoionization cross sections. Peak 5 is too close to the binding energy to be a double excitation.

E. General

What stands out most clearly after examination of the data on these gases is that all the large-amplitude structure can be semiquantitatively accounted for by the single conceptual scheme expounded by Dehmer[15,16] and his colleagues. One can deal with single-electron transitions and explain very strong features below and above the ionization threshold. It is necessary however to compute the overlap integrals with a realistic treatment of the orbital geometries when atoms are close together.

The question whether multielectron, shake-up, or double excitation transitions are observable is more difficult. We know they occur with ~5%–20% probability in photoelectron spectroscopy where the incoming photon energy is much greater than the binding energy. Also we know that shake-off probability decreases to zero as the photon energy decreases toward threshold. We do not know in general how the shake-up probability varies with excitation energy. Our interpretation in this paper has been that the shake-up probability will be small because it is a second-order process. The O_2 data support this interpretation, but it ought not to be pushed too far. Until an adequate theoretical formulation becomes available we will have to admit that some or all of the small broad peaks we see in the photoionization continuum could be due to double excitations and shake-up.

On the other hand, one may be able to explain all observations up to the present level of sensitivity entirely in one-electron terms. Whether the weak observed bumps arise from double excitation and shake-up (many electron) or from molecular modulation of the partial one-electron photoionization cross sections will have to be decided by future calculations. More data on the shake-up probabilities as the excitation energy is reduced to threshold are clearly needed.

The distinction between continuum shape resonances, molecular EXAFS, and "ordinary" EXAFS can easily be lost. One usually thinks of ordinary EXAFS as Kronig or Koessel structure at $\gtrsim 100$ eV above the ionization threshold caused by scattering of the outgoing p-wave electron under the

influence of the core hole. The continuum shape resonance is a peculiarly molecular effect that comes out strong because of the anisotropy of the molecular field which causes mixing of higher angular momentum l waves. However, all intermediate structure in the continuum occurs in various molecular and solid environments. As more data accumulate there will be a need for a better classification scheme.

V. CONCLUSIONS

Data on photoabsorption coefficients (cross sections) in the region of the oxygen K-edge have been obtained on four gases. Common characteristics of the spectra lead to four useful conclusions. (i) The dominant photoabsorption features can all be understood as one-electron transitions with a distribution of oscillator strength that can be explained through molecular-orbital calculations. (ii) Multielectron processes are probably present in the weaker features observed at $\lesssim 10\%$ of the total photoionization cross section. (iii) The simple diatomic molecule CO is a good test case for further calculations because it contains a well-defined continuum resonance. (iv) Oxygen is a good diatomic test case for calculations of inner-well discrete states.

The quantitative nature of the measured data also leads to conclusions about absorption coefficients of materials in different forms. (a) In the region within ~5 Ry above the ionization threshold of light elements it is not possible to extract accurate atomic absorption coefficients (cross sections) from measurements made on molecular gases or solids. Measurements made at discrete energies within ~5 Ry of an absorption edge should never be used for construction of smooth curves of atomic absorption. (b) Future tabulations of low-energy absorption coefficients for general use should be specific to compounds and physical state rather than to elements in atomic form.

ACKNOWLEDGMENTS

We thank C. E. Brion, D. C. Cartwright, J. L. Dehmer, B. L. Henke, A. P. Hitchcock, W. F. Heubner, P. W. Langhoff, and R. C. Martin for discussions on atomic processes and helpgul comments on the manuscript. This project was supported by the Department of Energy, Los Almos Scientific Laboratory and by NASA Grant No. S-57094-A.

---

*Present address: National Bureau of Standards, Washington, D.C. 20234.
†Present address: Univ. of Colorado, Boulder, CO 80302.
‡Present address: Univ. of New Mexico, Albuquerque, NM 87106.

[1]R. L. Blake, *Advances in X-Ray Analysis* (Plenum, New York, 1970), Vol. 13, p. 352.
[2]R. E. LaVilla, J. Chem. Phys. 63, 2733 (1975).
[3]B. L. Henke and E. S. Ebisu, *Advances in X-Ray Analysis* (Plenum, New York, 1973), Vol. 17, p. 150.
[4]M. Nakamura, M. Sasanuma, S. Sato, M. Watanabe, H. Yamashita, Y. Iguchi, A. Ejiri, S. Nakai, S. Yamaguchi, T. Sagawa, Y. Nakai, and T. Oshio, Phys. Rev. 178 80 (1969).
[5]M. Nakamura, Y. Morioka, T. Hayaishi, E. Ishiguro, and M. Sasanuma, Third International Conference on Vacuum Ultraviolet Radiation Physics, Tokyo, Japan, 1971 (unpublished), p. 1, p. A1–6.
[6]M. Barber, J. A. Connor, and I. H. Hillier, Chem. Phys. Lett. 9, 570 (1971).
[7]A. S. Vinogradov, B. Shlarbaum, and T.M. Zimkina, Opt. Spectrosc. 36, 383 (1974).
[8]G. R. Wight, C. E. Brion, and M. J. Van Der Wiel, J. Electron Spectrosc. Relat. Phenom. 1, 457 (1972, 1973).
[9]G. R. Wight and C. E. Brion, J. Electron Spectrosc. Relat. Phenom. 3, 191 (1974); 4, 313 (1974).
[10]C. J. Allan, U. Gelius, D. A. Allison, G. Johansson, H. Siegbahn, and K. Siegbahn, J. Electron Spectrosc. Relat. Phenom. 1, 131 (1972, 1973).
[11]F. C. Brown, R. Z. Bachrach, and A. Bianconi, Chem. Phys. Lett. 54, 425 (1978).
[12]A. Bianconi, H. Peterson, F. C. Brown, and R. Z. Bachrach, Phys. Rev. A 17, 1907 (1978).
[13]V.I. Nefedov, J. Struc. Chem. USSR 11, 277 (1970).
[14]T. M. Zimkina and A. S. Vinogradov, J. Phys. (Paris) 32, C4-3 (1971).
[15]J. L. Dehmer, J. Chem. Phys. 56, 4496 (1972).
[16]J. L. Dehmer and D. Dill, Phys. Rev. Lett. 35, 213 (1975); J. Chem. Phys. 65, 5327 (1976).
[17]J. S. Thomson, *X-Ray Spectroscopy*, edited by L. V. Azaroff (McGraw-Hill, New York, 1974), p. 26.
[18]L. G. Parratt, C. F. Hempstead, and E. L. Jossem, Phys. Rev. 105, 1228 (1957).
[19]A. J. Burek, Space Sci. Instrum. 2, 53 (1976).
[20]T. Magnusson, Nova Acta Regiae Soc. Sci. Ups. 11, No. 3 (1938).
[21]R. L. Blake and T. Passin, *Advances in X-Ray Analysis* (Plenum, New York, 1971), Vol. 14, p. 293.
[22]K. Siegbahn, C. Nordling, G. Johansson, J. Hedman, P. F. Heden, K. Hamrin, U. Gelius, T. Bergmark, L. O. Werme, R. Manne, and Y. Baer, *ESCA Applied to Free Molecules* (North-Holland, Amsterdam, 1969).
[23]S. Bodeur, C. Senemaud and C. Bonnelle, *Proceedings of the Fourth International Conference on Vacuum Ultraviolet Radiation Physics, Hamburg, 1974* (Pergamon, New York, 1974), p. 94.
[24]B. L. Henke and R. L. Elgin, in Ref. 1, Vol. 13, p. 639.

[25]E. J. McGuire, Phys. Rev. 175, 20 (1968).
[26]W. J. Veigele, At. Data 5, 51 (1973).
[27]A. Gerwer and B. V. McKoy (private communication).
[28]N. Padial, G. Csanak, B. V. McKoy, and K. W. Langhoff, J. Chem. Phys. 69, 2992 (1978).
[29]T. N. Rescigno and P. W. Langhoff, Chem. Phys. Lett. 51, 65 (1977).
[30]H. W. Schnopper, Phys. Rev. 131, 2558 (1963).
[31]F. Wuilleumier, J. Phys. (Paris) 32, C4-88 (1971).
[32]T. A. Carlson, W. E. Moddeman, and M. O. Krause, Phys. Rev. A 1, 1406 (1970).
[33]E. E. Salpeter and M. H. Zaidi, Phys. Rev. 125, 248 (1962).
[34]F. Wuilleumier and M. O. Krause, Phys. Rev. A 10, 242 (1974).
[35]T. A. Carlson, M. O. Krause, and W. E. Moddeman, J. Phys. (Paris) 32, C4-76 (1971).
[36]W. C. Price, A. W. Potts, and D. G. Streets, *Electron Spectroscopy*, edited by D. A. Shirley (American Elsevier, New York, 1972), p. 187.
[37]F. Wuilleumier and M. O. Krause, in Ref. 36, p. 259.
[38]U. Gelius, J. Electron Spectrosc. Relat. Phenom. 5, 985 (1974).
[39]T. Gustafsson, Phys. Rev. A 18, 1481 (1978).
[40]A. P. Hitchcock and C. E. Brion in an unpublished preprint show the high quality data on cross-section structure that electron scattering provides.
[41]R. B. Kay, Ph.E. Van der Leeuw, and M. J. Van der Weil, J. Phys. B 10, 2313 (1977).